The Effect of Hot Isostastic Pressing on the Optical Properties Of Spinel

Gary Gilde
410-306-0923
ggilde@arl.army.mil

Report Documentation Page

Form Approved
OMB No. 0704-0188

1. REPORT DATE	2. REPORT TYPE	3. DATES COVERED
20 MAY 2004	**N/A**	**-**

4. TITLE AND SUBTITLE	5a. CONTRACT NUMBER
The Effect of Hot Isostastic Pressing on the Optical Properties Of Spinel	5b. GRANT NUMBER
	5c. PROGRAM ELEMENT NUMBER
6. AUTHOR(S)	5d. PROJECT NUMBER
	5e. TASK NUMBER
	5f. WORK UNIT NUMBER
7. PERFORMING ORGANIZATION NAME(S) AND ADDRESS(ES) **U.S. Army Research Laboratory, Attn. AMSRL-WM-MC Aberdeen Proving Ground, MD 21005**	8. PERFORMING ORGANIZATION REPORT NUMBER
9. SPONSORING/MONITORING AGENCY NAME(S) AND ADDRESS(ES)	10. SPONSOR/MONITOR'S ACRONYM(S)
	11. SPONSOR/MONITOR'S REPORT NUMBER(S)

12. DISTRIBUTION/AVAILABILITY STATEMENT
Approved for public release, distribution unlimited

13. SUPPLEMENTARY NOTES
See also ADM201976, 10th DoD Electromagnetic Windows Symposium. Held in Norfolk, Virginia on 18-20 May 2004. , The original document contains color images.

14. ABSTRACT

15. SUBJECT TERMS

16. SECURITY CLASSIFICATION OF:			17. LIMITATION OF ABSTRACT	18. NUMBER OF PAGES	19a. NAME OF RESPONSIBLE PERSON
a. REPORT	b. ABSTRACT	c. THIS PAGE			
unclassified	**unclassified**	**unclassified**	**UU**	**17**	

The Effect of Hot Isostastic Pressing on the Optical Properties Of Spinel

Gary Gilde, Parimal Patel, and Philip Patterson
U.S. Army Research Laboratory, Attn. AMSRL-WM-MC
Aberdeen Proving Ground, MD 21005

David Blodgett, Donald Duncan, and Daniel Hahn
The Johns Hopkins University Applied Physics Laboratory
Laurel, MD 20723

Abstract

The effect of different hot isostatic pressing (HIP) temperatures and pressures on the optical transmission of hot pressed spinel was studied. The transmittance and extinction coefficient were measured. The transmittance data was used to determine the relative size of the scattering sites. HIP temperatures as low as 1500°C were seen to be effective in increasing the transmittance. The transmittance increased with increasing HIP temperature and pressure. The size of the scattering sites were large relative to the wavelengths of light measured. Interestingly the size of the scattering site was found to increase with increasing HIP temperature and pressure.

I. Introduction

Optically clear ceramics must be fully dense and free of any pores on inclusions which will scatter light. Sintering a ceramic to this high density with out the aide of sintering aids that leave residual second phases is very difficult. The application of pressure during HIPing is a way of increasing the density without aiding sintering aids that may leave second phases to act as scattering sites. To reduce the cost of HIPing it is desirable to HIP at the lowest temperatures and pressures possible

II. Experimental Procedure

Three spinel circular billets 100 mm in diameter, 10 mm thick were hot-pressed. The hot-pressing pressure for all three billets was 20 MPa. The hot-pressing matrix used to prepare the samples for these experiments is shown in Table I. The three billets were polished to an optical finish by NU-TEX Precision Optical Corporation, Aberdeen, MD. From each billet, 6 pieces, each 25 mm diameter and 6 mm thick, were core drilled. These pieces were then HIPed for 6 hours at (1)1500ºC/100 MPa, (2)1500ºC/200 MPa, (3)1700ºC/100 MPa, (4)1700ºC/200 MPa, and (5)1900ºC/200 MPa(Table II). One piece (0) was kept in the as hot-pressed condition to be used as a control.

Table I. Hot-Pressing Matrix

Sample	Hot pressing pressure	Firing conditions
A	20 MPa	1620ºC, 3 hrs
B	20 MPa	1650ºC 3 hrs
C	20 MPa	1650ºC 3 hrs: 1550ºC 12hrs vacuum anneal

Table II. Hot Isostatic Pressing Matrix

HIP ID #	HIP Pressure	HIP Temperature
0 control	-	-
1	100 MPa	1500ºC
2	200 MPa	1500ºC
3	100 MPa	1700ºC
4	200 MPa	1700ºC
5	200 MPa	1900ºC

Transmittance measurements were performed both with a conventional broadband spectrometer and two different Helium-Neon (HeNe) laser sources (632.8 nm and 3.39 μm). The spectrometer has the advantage of providing broad spectral transmittance measurements, but lacks the accuracy of some more direct measurements. Laser measurements, on the other hand, provide excellent accuracy at one frequency, but lack the spectral information of broadband approaches. Therefore, the combination of these two is synergistic.

Broadband transmittance measurements were performed from 500 nm to 7 μm using a Fourier Transform Spectrometer (BOMEM DA3.02) configured with a quartz-halogen lamp, quartz beamsplitter, and a silicon (Si) detector for the visible spectrum (500 to 800 nm). An MCT detector with a KBr beamsplitter and globar source were used for the mid-IR measurements (2 to 7 μm). The entire optical path of the spectrometer could be either evacuated or purged. Both visible and mid-IR measurements were collected in the purge mode to minimize time between reference and sample spectra and improve baseline stability and accuracy. The mid-IR measurements were then repeated in evacuation mode to remove water absorption lines and then scaled, if necessary, to match the results obtained in purge mode. Vacuum levels in the sample compartment between 0.08 and 0.5 Torr were typical.

The ultraviolet spectra between 180 nm and 500 nm were measured on a spectrometer (Cary 5G UV/VIS/NIR, VARIAN) set to scan from 185 nm to 400 nm at a rate of 500 nm/m. A holminium oxide reference filter was used to verify the spectrometer's performance. Before each sample analysis a background spectrum was collected as part of the instrument's baseline correction routine.

Laser measurements of transmittance were made at two HeNe laser wavelengths. Measurements at 632.8 nm used a chopped beam and a Si detector with an acceptance angle of 0.7° while measurements at 3.39 um used an InSb detector with an acceptance angle of 0.7°. The transmittance was determined by taking the ratio of the transmitted power through a sample, I_t, with the incident laser power without a sample, I_0. These two measurements allow for the total extinction coefficient, β_e, to be determined. Since the measurements were made in regions where no intrinsic absorption occurs, the total extinction was completely attributed to scatter.

Optical phase functions representing the angular distribution of the scatter were performed to determine the bi-directional scatter distribution functions (BSDF). These measurements were performed with the visible HeNe laser. For the BSDF measurements, the source laser beam was chopped, expanded, and focused onto a detector mounted on a rail, which was in turn mounted on a rotational stage. The detector was rotated around the sample and the detector output recorded by a lock-in amplifier whose reference signal was derived from the chopper. The sample was mounted at the center of rotation of the detector-rail system and at a near-normal angle of incidence with respect to the incident beam. This provides complete characterization of the scatter intensity profile for each of the samples. For these measurements, polarization was ignored and we assumed that the scattered light is independent of sample rotation about the sample normal.

III. Results

Single wavelength laser estimates of the total extinction coefficient, β_e, are obtained from the transmittance measurements. Measurement of the transmittance, T, coupled with knowledge of the sample thickness, L, and refractive index, n, allows the extinction coefficient to be determined as follows

$$\begin{aligned} T &= \frac{I_t}{I_0} = \frac{(1-R)^2}{\left(1-R^2 e^{-2\beta_e L}\right)} e^{-\beta_e L}, \quad \text{and} \\ R &= \left(\frac{n-1}{n+1}\right)^2. \end{aligned} \tag{1}$$

The refractive index, as determined from a Sellmeier model[1], is 1.7137 at 632.8nm and 1.6376 at 3.39μm. These values are not expected to vary between the different spinel samples as variations in transmittance are attributed to scattering. From Eq. 1, the total extinction coefficient can be calculated as

$$\beta_e = \frac{\ln\left[2R^2T\right] - \ln\left[\sqrt{(1-R)^4 + 4R^2T^2} - (1-R)^2\right]}{L}. \tag{2}$$

Figure 1 shows a comparison of the measured visible and infrared transmittance as a function of the various HIP conditions for the three different hot-pressed billets. Tables I and II detail the conditions for the hot-pressing (A, B, C) and the HIPing (1-5). Samples (A, B, C) with a 0 designation were a control and were only hot-pressed. These results show that the HIP process even at the lowest temperature and pressure greatly improves the optical properties of the samples. Samples A and C showed almost a constant improvement in the visible transmittance for the five HIP processing conditions. This improvement is not seen in the infrared measurements, where transmittance approaches the theoretical limit for all HIP

conditions. Both the visible and infrared transmittances of sample B remained relatively constant for HIP temperatures, with only a small improvement found at the highest HIP pressure and temperature (ID#5). It is interesting to note that increasing the HIP pressure from 100 MPa to 200 MPa while maintaining the HIP temperature at 1500°C slightly degraded the optical properties of two of the samples (B and C). Table III shows a comparison of the determined transmittance and extinction coefficient. The uncertainty in these measurements is about 0.001 for the transmittance and 0.02 cm^{-1} for the extinction coefficient.

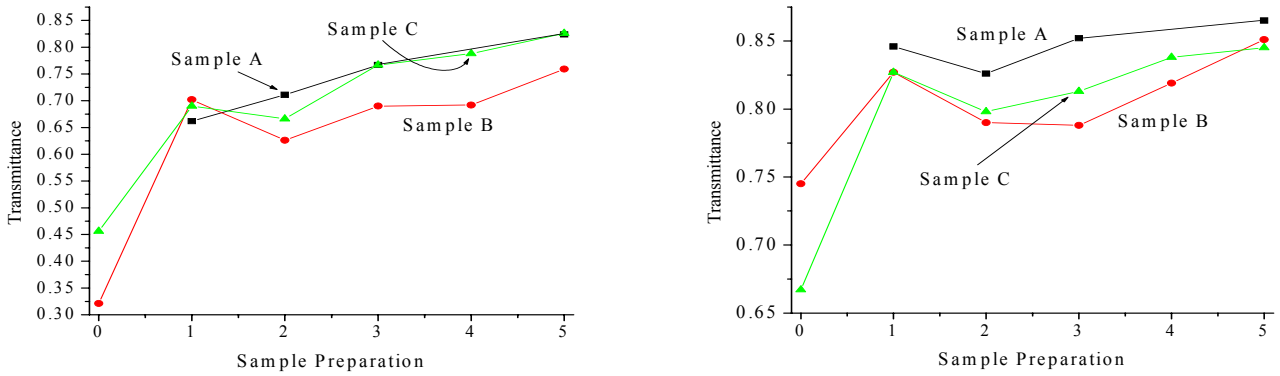

Fig. 1. Dependence of a) visible (632.8 nm) and b) infrared transmittance (3.39 μm) of three different billets (A, B, C) HIPed at various conditions (1,2,3,4,5). Sample 0 is a control and is only hot-pressed.

Table III. Comparison of Measured Transmittance and Extinction Coefficients

Sample	Length [cm]	Visible (632.8 nm)		Infrared (3.39 μm)	
		T ±0.001	β_e [cm^{-1}] ±0.02	T ±0.001	β_e [cm^{-1}] ±0.02
A1	0.517	0.662	0.52	0.853	0.07
A2	0.521	0.711	0.39	0.833	0.11
A3	0.522	0.767	0.24	0.831	0.12
A5	0.521	0.824	0.10	0.866	0.04
B0	0.608	0.321	1.63	0.745	0.28
B1	0.519	0.702	0.41	0.827	0.13
B2	0.523	0.626	0.63	0.790	0.21
B3	0.517	0.690	0.45	0.788	0.22
B4	0.520	0.692	0.44	0.819	0.15
B5	0.520	0.759	0.26	0.851	0.07
C0	0.613	0.477	0.98	0.795	0.17
C1	0.520	0.690	0.44	0.827	0.13
C2	0.522	0.666	0.50	0.798	0.20
C3	0.524	0.767	0.24	0.813	0.16
C4	0.516	0.788	0.19	0.838	0.10
C5	0.524	0.826	0.10	0.845	0.09

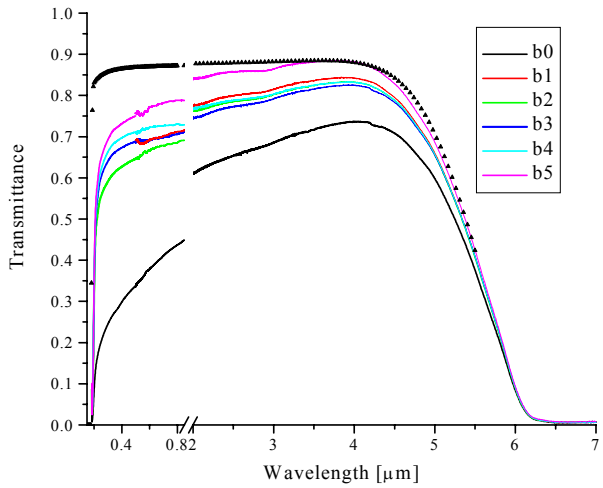

Fig. 2. Comparison of the intrinsic (symbol) and measured transmittance properties for a hot-pressed billet B as a function of HIP conditions in the UV, visible, and IR spectrum.

Shown in Fig. 2 is the transmittance spectrum for sample B specimens as a function of HIP conditions, from 185 nm through 7 μm. Samples A and C follow similar trends. After the lowest HIP treatment at 1500C and 100MPa there is very little difference between samples A, B and C. There is some discontinuity at 500 nm due to transition between the two different spectrometers (185nm - 500 nm & 500 nm- 850nm). Discrepancies between the laser transmittance (see Table III) and spectrometer data at 632.8 nm and 3.39 μm (see Fig. 2) are attributed to differences in the field of view (FOV) for the different instruments. The optical detectors for the laser transmittance measurements have a
FOV of 0.7° while the visible/IR spectrometer has a FOV of 7.125°. Therefore, the spectrometer collects a substantial portion of the scattered light. As shown in the BSDF plots in Figure 3, there is a significant amount of scatter in both the B0 and C0 samples. Integrating the BSDF plots over the FOV of the BOMEM as follows

$$T = \int_0^{2\pi} d\phi \int_{-\theta_{FOV}}^{\theta_{FOV}} BSDF(\theta)\sin(\theta)\,d\theta \qquad (3)$$

yields transmittance values of 0.37 and 0.52 for the B0 and C0 samples that agree well with the transmittances measured in the BOMEM (0.36 and 0.51, respectively). Also included in the figure is the calculated intrinsic transmittance of spinel. The calculated transmission is based on the Sellmeier model for the real part of the refractive index and then includes both the Urbach tail in the UV and IR absorption edge for the imaginary portions of the refractive index. This complex refractive index is then used in Equation 1 to calculate the intrinsic transmittance.

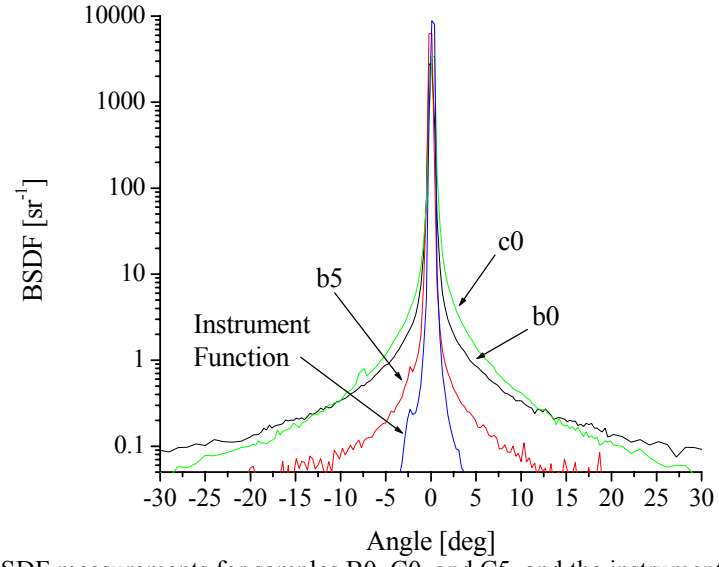

Fig. 3. Comparison of BSDF measurements for samples B0, C0, and C5, and the instrument function.

Referring to Fig. 2, one sees that the as-is hot pressed samples exhibited substantially lower transmittances particularly in the UV and visible spectrums where optical scattering dominates. The transmission of the hot pressed samples is greatly increased by annealing in vacuum for 12 hours at 1550°C (sample C0). The samples hot-pressed at 1620°C (A0) and 1650°C (B0) have a transmittance of about 0.38 at 633nm while the sample hot-pressed at 1650°C and then annealed at 1550°C for 12 hours (C0) had a transmittance of almost 0.53. As with the optical scattering measurements, it was found that hot-pressing at 1650°C versus 1620°C degrades the visible optical properties of the samples. This disparity is not as large in the infrared transmittance region. Annealing the samples after hot-pressing at 1650°C negates this effect.

Comparisons of the scatter distribution functions (BSDF) measured at 632.8nm, for three of the samples (B0, B5, and C0) and the instrument function of the BSDF system are shown in Fig. 3. The instrument function plot represents what an ideal sample, with no scatter, would be like. Of the three samples, sample B5 has the narrowest scatter profile, although it

is noticeably wider than the instrument function. The smaller scatter angle and higher peak of B5 as compared to B0 contributes to the higher transmittance values reported in Table III (0.759 vs. 0.321). It is interesting to note the effect that annealing has on the scatter profile of the hot pressed samples (C0 versus B0). The C0 sample has a slightly higher peak transmittance than B0, which is reflected in an increase in the measured transmittance from 0.477 over 0.321. The BSDF for C0 and B0 are slightly misleading. The β_e for C0 (0.80) is smaller than for B0 (1.45) although on the BSDF plot, C0 appears wider. However, the two curves cross at 11^o and the total area under the curve is greater for B0, consequently it has a larger β_e

Examination of the spinel using an optical microscope with transmitted light was instructive. In the as hot-pressed samples there were many decorated grain boundaries, triple points, and pore clusters. As the HIP temperature was increased the frequency of decorated grain boundaries, triple points, and pore clusters decreased. Optical micrographs from the as hot-pressed sample as well as samples HIPed at 1500°C, 1700°C and 1900°C are shown in Fig. 4. They clearly show that as the HIP temperature is increased the number of scattering sites decreases. After HIPing at 1900°C the microstructure is almost featureless. The size of the pores increases with increasing HIP Temperature. This is also shown in the scattering study where the power law relationship indicates that the size of the scattering site is increasing with increasing HIP temperature and pressure.

In an effort to better understand the scatter phenomena in the spinel, analysis of the transmittance data presented in Fig. 2 was performed. Equation 2 was used with the spectrometer data to obtain spectral estimates of the scatter cross-section per unit volume. Subsequently, a power law was used to fit to the ensuing estimate:

$$\beta_{\text{sca}} \propto \lambda^{-\nu} . \tag{4}$$

Inspection of the resulting exponent reveals information about the size, relative to the wavelength, of the structures responsible for scatter. In particular, if the wavelength is large with respect to the scatterers, one observes an exponent of four. This is referred to as the Rayleigh regime. On the other hand, when the scatterers are large in comparison to the wavelength, the exponent approaches zero. This is known as the geometrical optics regime. Shown in Fig. 5 is an example of such an analysis. Here we see that the exponents are on the order of unity, which is consistent with a transition between the Rayleigh and geometrical optics regimes. More importantly, however, is the trend for samples C1 through C5. The exponent consistently decreases with increasing HIP temperature and pressure. This suggests that as the HIPing proceeds, the structures responsible for scatter continually grow in size.

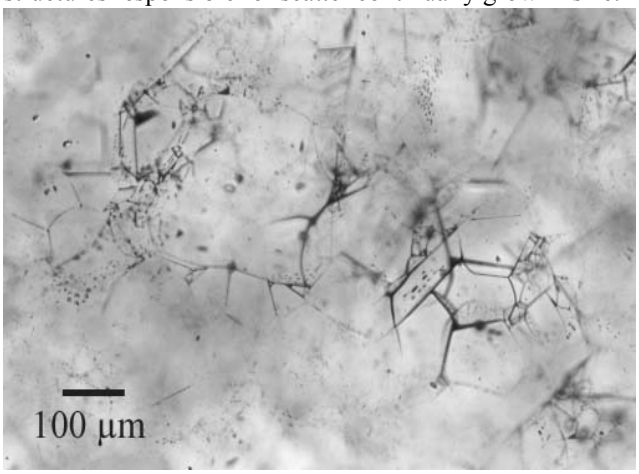

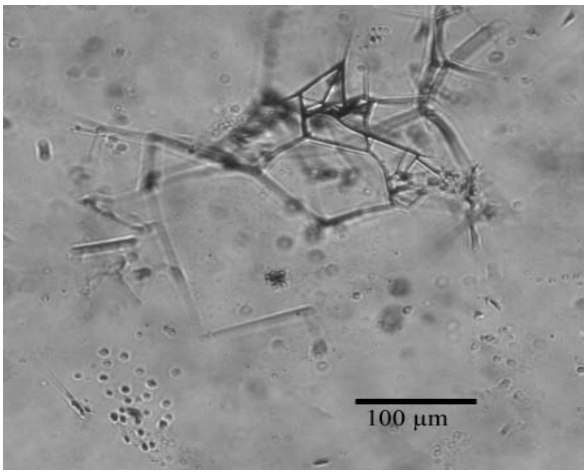

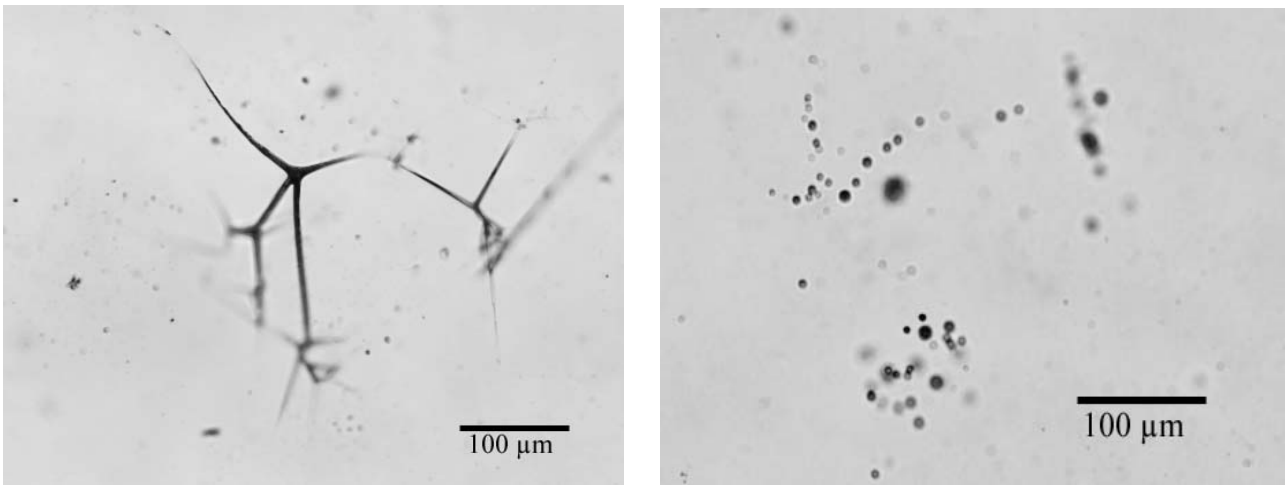

Figure 4. Optical Micrographs showing defects in spinel using transmitted light. Top Left as Hot pressed, Top Right HIped 1500°C, Bottom Left Hiped 1700°C, and Bottom Right Hiped 1900°C.

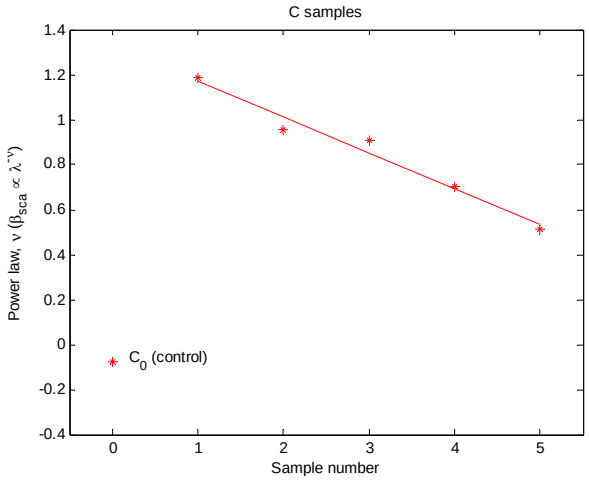

Figure. 5. Power law wavelength dependence of scatter cross-section for C samples

IV. Discussion

HIPing at temperatures and pressures as low as 1500°C/100MPa significantly increases the transmission of hot pressed spinel .even though this temperature is 120°C below the hot pressing temperature. This improvement is attributed to a decrease in the bulk scatter. In the mid-IR the scattering coefficient is reduced to about 0.15 cm^{-1} after HIPing at 1500°C/100MPa. HIPing at higher temperatures and pressures provides minimal benefit and will likely result in a lower strength material due to grain growth. At 632.8 nm, there is significant scatter until the samples were HIPed at 1900°C/200MPa. In the case of sample B5, scatter remains even after this HIP treatment. As can be seen in Fig. 1 and Table III, transmission generally remained constant or increased slightly with increasing HIP temperature. The effect of increasing pressure is less clear. In the UV, we found that the increasing pressure while holding the temperature fixed, resulted in an increase in transmission for 5 out of the 6 processing conditions. In the last case the transmission dropped with an increase in pressure. It is likely that this drop in transmission is not the result of increasing the HIPing pressure, but the result of sample-to-sample variation that was not evident in the visual inspection before core drilling the samples from the hot-pressed spinel samples. Based on our results the HIP temperature should be at least 1700°C, preferably 1900°C, to reduce the scatter for use in the visible portion of the spectrum. There is some scatter remaining after HIPing at 1700°C but this can probably be removed by optimizing the hot-pressing and annealing cycle. Sample C0, which was annealed, had lower scatter as hot-pressed compared to A0 and B0. Future work will look both at the effect of longer duration HIP cycles and improving the hot-pressing cycle.

Optical microscopy shows the presence of decorated grain boundaries, decorated triple points, and pore clusters. Pores were generally found in clusters. This would seem to indicate that they are result of agglomerates in the starting powder. The grain boundaries and triple points are decorated with LiF that was not removed during the hot-pressing cycle. These pore clusters and decorated triple points will act as scattering sites. The decorated grain boundaries may also increase

the scattering. HIPing seems to allow the LiF to continue to be removed and the number of pore clusters to be reduced. This is evidenced by the reduced scatter and can be seen in the micrographs. Results from the power law wavelength dependence show that the size of the scattering sites increases with increasing HIP temperature and pressure. Obviously the number of scattering sites decreases since the overall transmission and scattering coefficient decrease with increasing HIP temperature. The growth in scattering site size would indicate that pores will grow and could become large enough to become stable pores that will not be eliminated by further HIPing. Optimizing the hot-pressing and annealing schedules to eliminate more of the LiF and reduce the porosity will allow the HIP cycle to be more effective

V. Conclusions

The optical properties of spinel have been shown to be dependent on the HIP process conditions. Low temperature HIP cycles (1500°C) greatly increased the near and mid infra-red transmission of hot-pressed spinel. Higher temperatures are needed to improve transmission to the point where the hot-pressed spinel could be used in the visible and ultraviolet portion of the spectrum. The transmission increases with increasing HIP temperature and pressure. Spinel that was HIPed at 1900°C had a 82% transmission with a extinction coefficient of 0.1 measured at 632.8 nm.

The scattering sites are large relative to the wavelengths of light measured in this study. In the as hot-pressed material the scattering sites are pores and residual lithium fluoride at triple points and grain boundariers. As the HIP temperature is increased the LiF is less evident and the scattering is dominated by the remaining pores. These pores grow in size as the HIPing temperature and pressure is increased through pore coalescence. Because of this it is HIPing cannot remove all of the porosity. The hot-pressing schedule and powder processing, needs to be optimized to reduce or eliminate porosity during hot-pressing.

References

.Harris, D. C., Materials for Infrared Windows and Domes, Properties and Performance, SPIE Press, Bellingham, Washington, 1999.

M.E. Thomas, R.L. Joseph and W.J. Tropf, "Infrared Properties of Sapphire, Spinel and Yttria as a Function of Temperature", SPIE vol. 683, 1986.

J.A. Cox, D. Greenlaw, G. Terry, K. McHenry and L. Fielder, "Infrared and Optical Transmitting Materials", SPIE vol. 683, 1986

G. Gilde, P. Patel, M. Patterson, "A comparison of Hot-Pressing, Rate controlled Sintering and Microwave Sintering of Magnesium Aluminate Spinel for Optical Applications", Window and Dome Technologies and Materials VI, R.W. Tustison, Volume 3705, 1999 Proceedings of SPIE, Washington, USA

D.W. Roy, M. C.L. Patterson, J. E. Caiazza, G. Gilde, "Progress In Development Of Large Tansparent Spinel Plates", Proceedings 8th DoD Electromagnetic Windows Symposium, April 2000

The effect of Hot Isostastic Pressing on the Optical Properties of Spinel

Gary Gilde, Parimal Patel, and Philip Patterson
U.S. Army Research Laboratory, Attn. AMSRL-WM-MC
Aberdeen Proving Ground, MD 21005

David Blodgett, Donald Duncan, and Daniel Hahn
The Johns Hopkins University Applied Physics Laboratory
Laurel, MD 20723

Home

Agenda

Hot-Pressing and Hot Isostatic Pressing Matrix

Sample	Hot pressing pressure	Firing conditions
A	20 MPa	1620C, 3 hrs
B	20 MPa	1650C, 3 hrs
C	20 MPa	1650C, 3 hrs:1550C 12 hr vacuum anneal

HIP ID #	HIP Pressure	HIP Temperature
0 control	-	-
1	100 Mpa	1500C
2	200 MPa	1500C
3	100 MPa	1700C
4	200 MPa	1700C
5	200 MPa	1900C

Dependence of (A) visible (632.8 nm) and (B) Infrared Transmittance (3.39 mm)

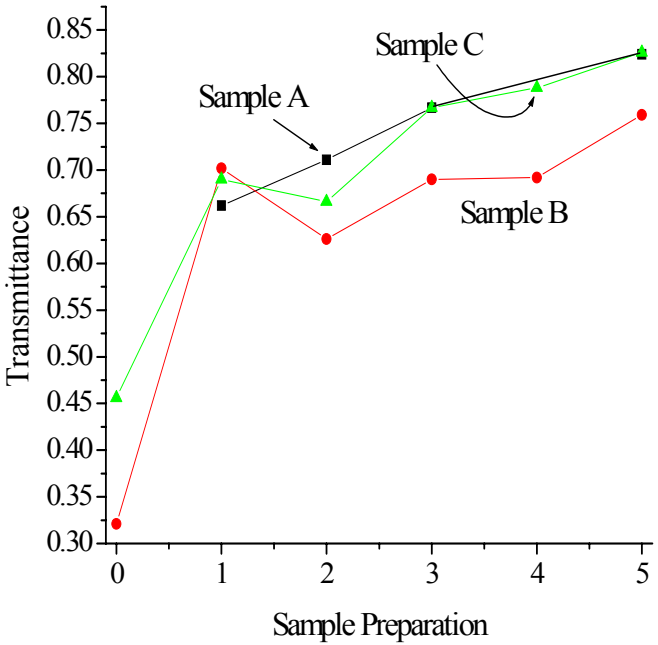

A.

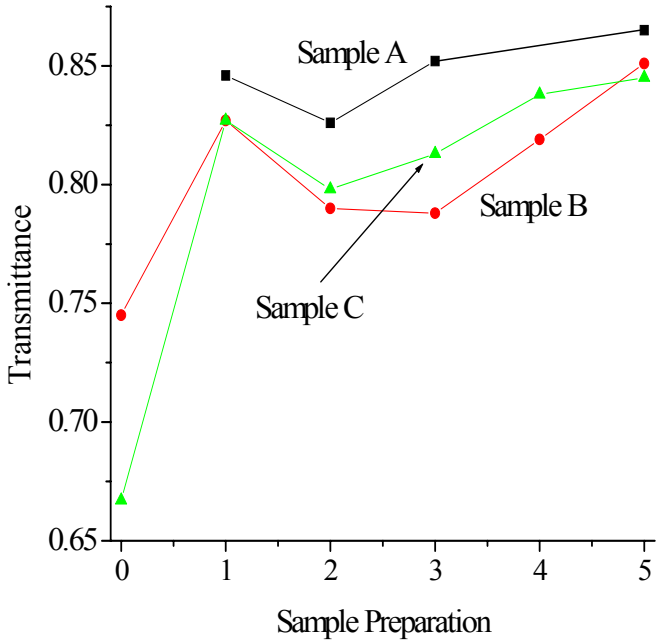

B.

Comparison of Measured Transmittance and Extinction Coefficients

Sample	Thickness (cm)	Transmission 632.8 nm	Extinction Coefficient	Transmission 3.39 um	Extinction Coefficient
A1	0.517	0.662	0.52	0.853	0.07
A2	0.521	0.711	0.39	0.833	0.11
A3	0.522	0.767	0.24	0.831	0.12
A5	0.521	0.824	0.10	0.866	0.04
B0	0.608	0.321	1.63	0.745	0.28
B1	0.519	0.702	0.41	0.827	0.13
B2	0.523	0.626	0.63	0.790	0.21
B3	0.517	0.690	0.45	0.788	0.22
B4	0.520	0.692	0.44	0.819	0.15
B5	0.520	0.759	0.26	0.851	0.07
CO	0.613	0.477	0.98	0.795	0.17
C1	0.520	0.690	0.44	0.827	0.13
C2	0.522	0.666	0.50	0.798	0.20
C3	0.524	0.767	0.24	0.813	0.16
C4	0.516	0.788	0.19	0.838	0.10
C5	0.524	0.826	0.10	0.845	0.09

Comparison of the Intrinsic and Measured Transmittance Properties for Billet B

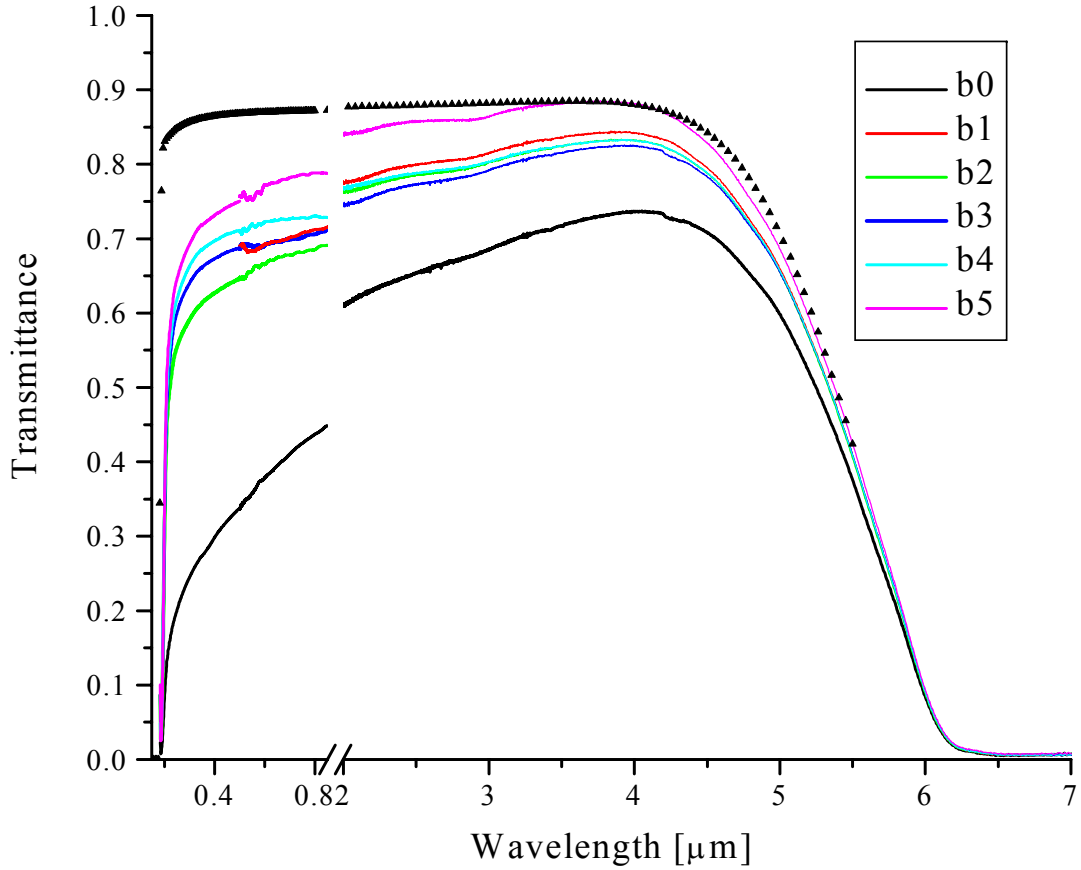

Comparison of BSDF Measurements for Samples B0, C0, and C5, and the Instrument Function

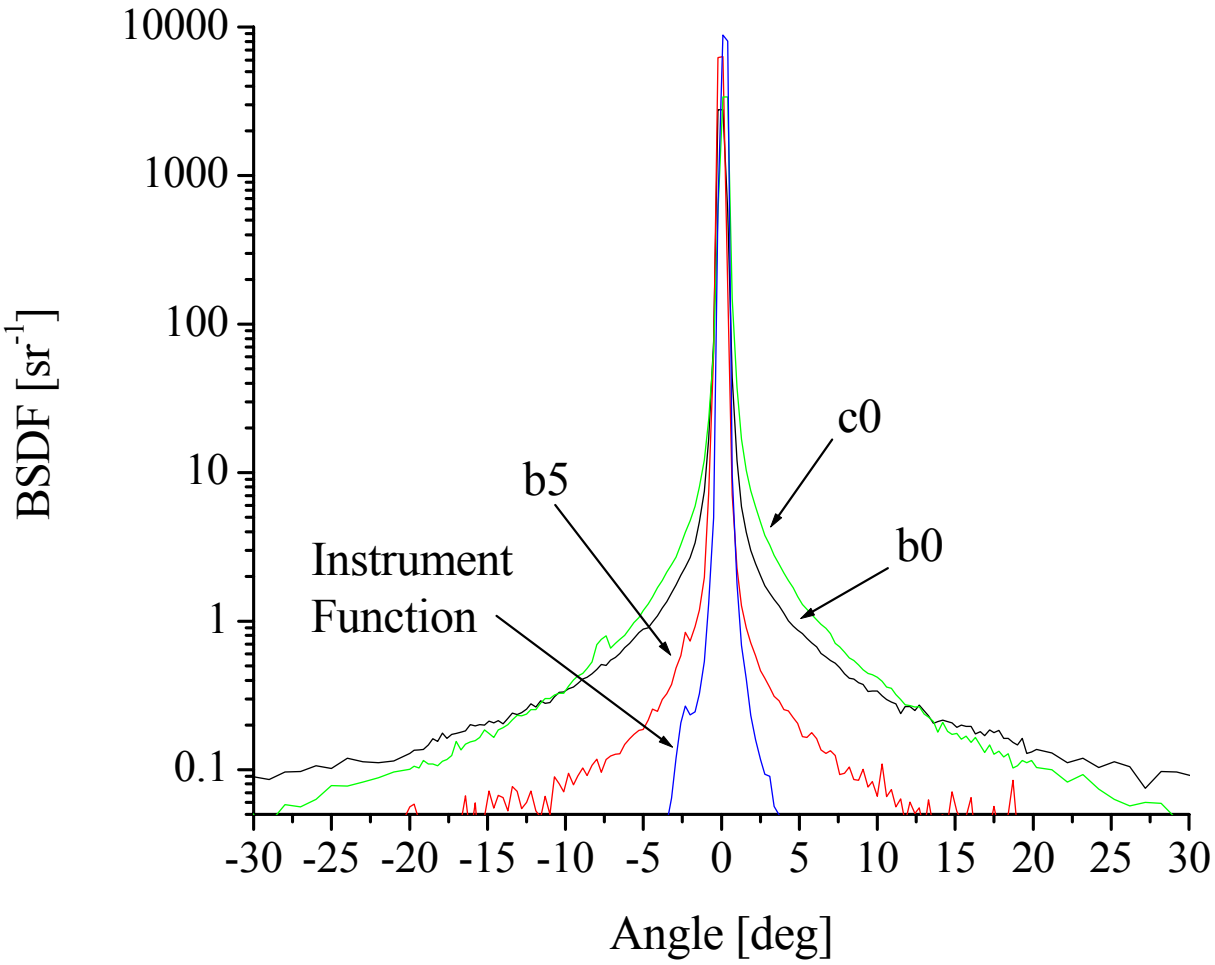

Power Law Wavelength Dependence of Scatter Cross-Section for C Samples

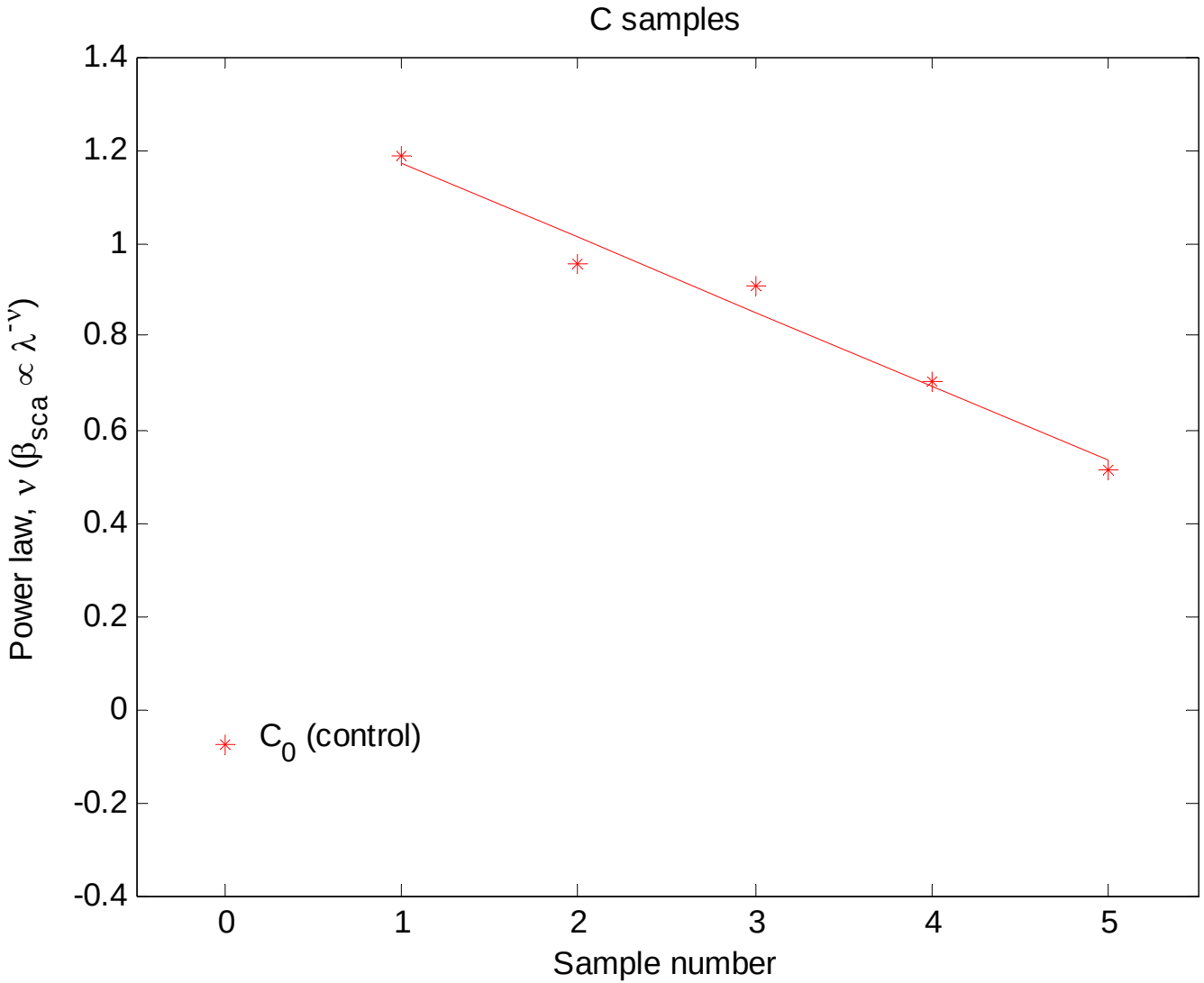

Typical Spinel Defects as a Function of HIP Temperature

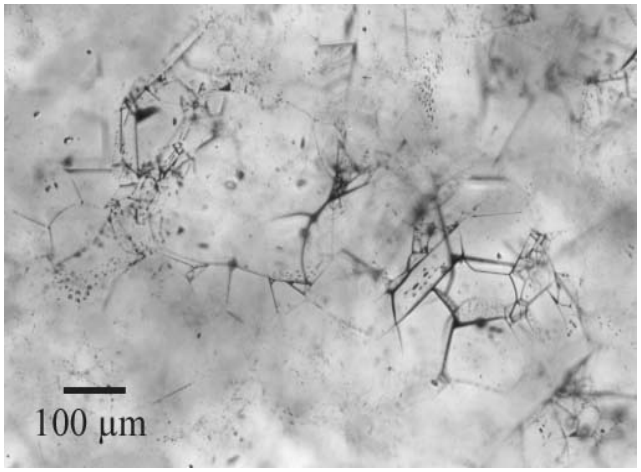

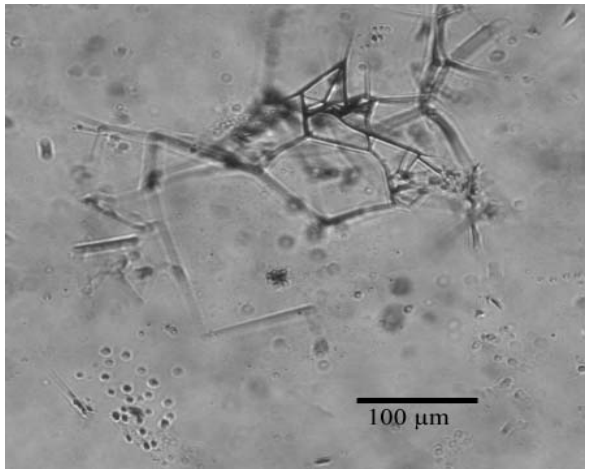

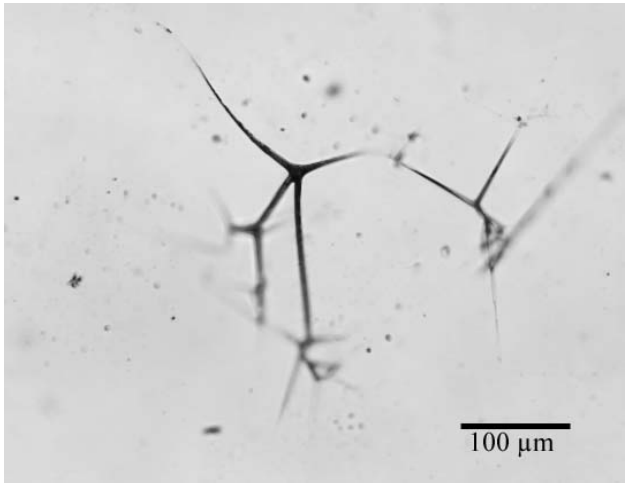

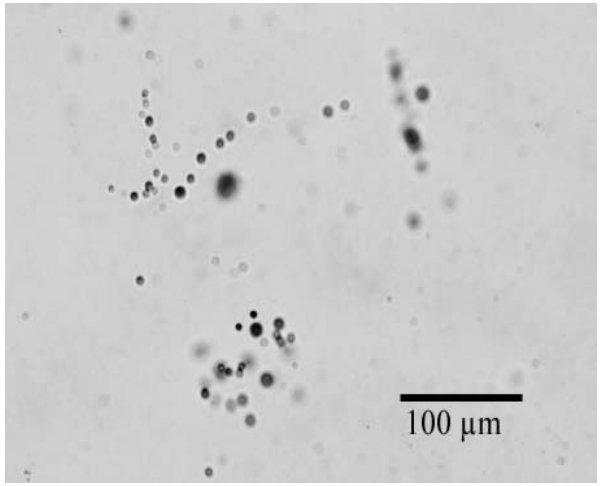

Optical Micrographs showing defects in spinel using transmitted light.
Top Left as Hot pressed, Top Right HIped 1500°C, Bottom Left
Hiped 1700°C, and Bottom Right Hiped 1900°C.